

# Development of microelectromechanical deformable mirrors for phase modulation of light

**Raji Krishnamoorthy Mali**, MEMBER SPIE  
**Thomas G. Bifano**  
**Nelsimar Vandelli**  
Boston University  
Department of Aerospace and Mechanical  
Engineering  
Boston, Massachusetts 02215  
E-mail: raji@engc.bu.edu

**Mark N. Horenstein**  
Boston University  
Department of Electrical and  
Computer Engineering  
Boston, Massachusetts 02215

**Abstract.** A silicon-based, surface micromachined, deformable mirror device for optical applications requiring phase modulation, including adaptive optics and pattern recognition systems is described. The mirror will be supported on a massively parallel system of electrostatically controlled, interconnected microactuators that can be coordinated to achieve precise actuation and control at a macroscopic level. Several generations of individual actuators as well as parallel arrays of actuators with segmented/continuous mirrors have been designed, fabricated, and tested. Deflection characteristics and pull-in behavior of the actuators have been closely studied. Devices have been characterized with regard to yield, repeatability, and frequency response. An electromechanical model of the system has been simulated numerically using the shooting method, and good correlation with experimental results has been obtained. A twenty-channel parallel control scheme has been developed and implemented on a segmented mirror array. © 1997 Society of Photo-Optical Instrumentation Engineers.

Subject terms: deformable mirrors; microelectromechanical systems; adaptive optics.

Paper 38046 received April 29, 1996; revised manuscript received Sep. 18, 1996; accepted for publication Sep. 20, 1996.

## 1 Introduction

Silicon-based microsystem components have recently received much attention in the optics field because they have many attractive features that make them suitable for optical applications. These devices have dimensions comparable with the wavelength of light, and can be easily and inexpensively batch fabricated in massive arrays of elements. They can be made from a variety of materials and have smooth, optical-quality surfaces. In addition, since they have low inertia, they can be positioned accurately with small forces, even at high frequencies.

Some of the significant optical applications of microelectromechanical systems (MEMS) technology arise from the ability to organize individual microactuators into arrays that cooperatively perform a macroscopic function. A prominent example of MEMS successfully applied to arrays of interconnected microactuators is the digital projection display<sup>1</sup> based on the digital micromirror device (DMD) built by Texas Instruments. The torsion mirror used in this display is a bistable device, capable of tilting  $\pm 10$  deg to reflect incoming light in one of two directions. The DMD technology has also been used in several other applications, including coherent optical correlators<sup>2,3</sup> and spatial light modulators.<sup>4</sup> Bulk micromachined deformable mirrors have been reported for spatial light modulation<sup>5,6</sup> and adaptive optics.<sup>7</sup>

## 2 MEMS Deformable Mirror

The deformable mirror system described here incorporates a continuous mirror sheet actuated at discrete points, the deformation being normal to the surface and continuous over a desired range. Figure 1 is a schematic showing a

cross section through three actuators in a row with a mirror sheet over them. The actuators are double cantilever beams, a structurally robust design. When voltage is applied between an actuator and the substrate or a ground pad, the electrostatic force developed deflects the actuator toward the substrate. The mirror sheet, which is attached to the actuator at midspan by a post, also deflects as a result. The amount of deflection depends monotonically but nonlinearly on the magnitude of the applied voltage. In the schematic, the actuator in the center is deflected, while the others are undeflected. The targeted applications for this MEMS deformable mirror include adaptive optical imaging and projection systems, and optical correlators for pattern recognition systems.

## 3 Adaptive Optics

Adaptive optics (AO) systems correct aberrations in an optical system through active control of mirror geometry. The most common AO systems use nominally flat, deformable secondary mirrors, whose shape is adjusted to compensate for aberrations in an optical wavefront. One important application of AO is compensation of aberration due to atmospheric turbulence in land-based astronomical telescopes. The process is called phase conjugation, and requires that each of the deformable mirror's many segments or zones be controlled in real time. Figure 2 shows the elements in a typical adaptive optics imaging system. The aberrated incoming wavefront is sent to a wavefront sensor (such as a Hartmann sensor), which analyzes the wavefront optically (for tilt and shape). The tilt signals control the tilt or steering mirror, and the shape signals are applied to a deform-

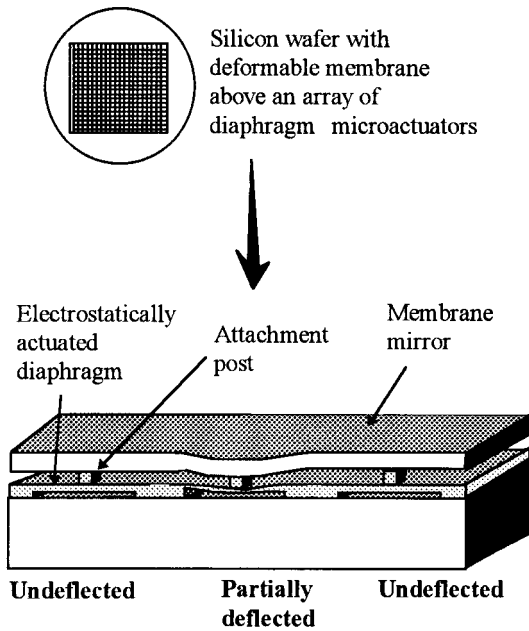


Fig. 1 Schematic cross section of a section of a deformable mirror array showing actuator deflection.

able mirror, generating a conjugate shape that corrects the aberration. With AO, the achievable image resolution is greatly enhanced.

Sophisticated adaptive optics systems have applications in astronomy for increasing light-gathering power and improving the angular resolution of large observatory telescopes.<sup>8</sup> Adaptive optics compensation is also used in laser communications and high-energy laser applications such as laser fusion to maintain beam collimation or improve beam focus. In space applications, AO helps compensate for gravitational effects. Small, light, and inexpensive MEMS-based deformable mirror systems will enable adaptive optics image enhancement for an entirely new range of commercial and scientific applications. Some op-

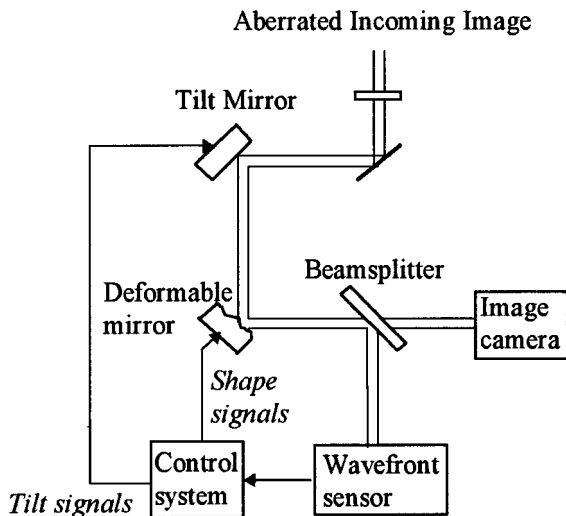


Fig. 2 Elements of a typical adaptive optical imaging system.

tical systems that could be affected include mid-sized astronomical telescopes, earth-satellite communication systems, industrial laser focusing, land-based optical telescope or binocular imaging systems, and biomedical imaging systems.

### 3.1 Deformable Mirror Specifications Based on Adaptive Optics Requirements

The primary parameters of deformable mirror AO systems are the number of actuators, the control bandwidth, and the maximum actuator stroke. For astronomical observations, these design parameters can be estimated based on the desired Strehl ratio (the Strehl ratio,  $S$ , is a common measure of imaging performance; it is the ratio of on-axis intensity of an aberrated image to on-axis intensity of the unaberrated image), the optical wavelength of interest, the characteristics of the optical disturbance (e.g., intensity of atmospheric turbulence) and the optical system aperture, using theoretical turbulence and photonic models.

The number of actuators required for a system is determined by the nature of the aberration, the wavelength of interest, and the desired Strehl ratio. An estimate of the number of actuators required for correction of atmospheric turbulence in an imaging system is given by<sup>9</sup>:

$$N_a = \left[ \frac{\kappa k^2 z C_n^2 D^{5/3}}{2.9 \ln(1/S)} \right]^{6/5}, \quad (1)$$

where  $\kappa$  is the Kolmogorov fitting constant,  $k$  is the wave number of the incident irradiation,  $z$  is the altitude or propagation distance,  $C_n^2$  is the atmospheric structure constant,  $D$  is the aperture diameter of the optical system, and  $S$  is the desired Strehl ratio.

The stroke required of the mirror and therefore each actuator is determined by the expected range of the wavefront phase error. For optical imaging through atmospheric turbulence, the required phase excursion can be approximated as:

$$(\Delta\phi)_{\max} = 0.57k \sqrt{z C_n^2 D^{5/3}}. \quad (2)$$

The minimum control frequency required for each actuator can also be estimated, based on the rate at which the source of optical aberrations is changing. For correction of phase errors caused by atmospheric turbulence, the so-called Greenwood frequency can be determined by<sup>10</sup>:

$$f = \frac{0.4v}{\sqrt{\lambda L}}, \quad (3)$$

where  $v$  is the mean wind velocity in the turbulent layer,  $\lambda$  is the wavelength of the incident light, and  $L$  is the average thickness of the turbulent layer.

For example, based on assumptions of moderate turbulence, near-infrared light ( $\lambda = 1.0 \mu\text{m}$ ), a 1-m diameter primary mirror, and a Strehl ratio of 0.2, a deformable mirror would require 400 actuators, a closed-loop bandwidth of 20 Hz, and a stroke of  $2 \mu\text{m}$ . These parameters are the design goals for the MEMS deformable mirror under development. Deformable mirrors used in a phase-only filter application

also require high actuator density and  $\sim 2 \mu\text{m}$  stroke, but they can be operated open loop at low frequencies.

The time scale for variations in the distortion, the coherence time, is on the order of a few milliseconds at optical wavelengths. Phase error corrections must therefore be made within a few milliseconds of wavefront measurement to be effective. This in turn requires closed-loop control bandwidths up to 1 kHz. To achieve control at 1 kHz, the natural frequency of the actuator should be at least 10 kHz. The natural frequency for a continuous deformable mirror membrane driven by an array of discrete actuators is given by<sup>10</sup>:

$$f_n = \frac{10.21h}{2\pi R^2} \sqrt{\frac{E}{12\rho(1-\nu^2)}} \quad (4)$$

where  $h$  is the membrane thickness,  $R$  is the interactuator spacing,  $E$  is the elastic modulus of the membrane material,  $\rho$  is the membrane density, and  $\nu$  is the Poisson's ratio of the membrane. For the deformable mirror devices, predicted resonant frequencies are all in excess of 30 kHz, higher than any other deformable mirror system implemented to date.

### 3.2 Advantages of MEMS Deformable Mirrors

Currently available multichannel correction mirrors in AO systems include both segmented and continuous mirrors. Segmented mirrors offer advantages in terms of scalability, assembly, and maintenance. There is no cross-coupling between actuators, and systems with 512 segments operating at 5 kHz<sup>11</sup> have been implemented. However, the gaps between segments cause a reduction in performance as energy is lost through them, and the gaps act like a grating, causing energy to be diffracted from the central lobe. For higher-quality performance, continuous-surface deformable mirrors are used, with either continuous-membrane piezoelectric bimorph actuators<sup>12</sup> or independent piezoelectric actuators.<sup>13</sup> Discrete actuator deformable mirrors exhibit relatively higher spatial resolution and temporal response, and can be built for larger strokes. However, piezoelectric actuators have many problems, including the presence of hysteresis, inhomogeneous behavior over time, large operating voltage requirements, and large size. These systems are typically quite expensive (\$1000 per channel), heavy, and require an integral cooling system to eliminate excess heat.

MEMS deformable mirrors exhibit advantages over competing deformable mirror systems in performance, fabrication, and economy. They exhibit no hysteresis, making them easier to control. They operate using lower voltages (typically <100 V). Being electrostatically driven, they consume essentially no power, and their low-power operation reduces the cost of drive circuitry. They are lightweight and can be packaged closely in massively parallel arrays for higher spatial resolution. Consistent temporal performance and high-bandwidth operation (>66 kHz) have been achieved using electrostatic MEMS actuators of the size needed for this application, as described in this paper.

Fabrication is streamlined, no discrete assembly is required, and the device can be packaged in conventional integrated circuit (IC) packages with standard pin connec-

tors. System electronics could be integrated into the deformable mirror device although such integration is not essential. The proposed MEMS systems are inexpensive, with projected costs under \$10 per actuator for a 400-zone mirror at prototype stage. Since they use existing semiconductor fabrication technology and can take advantage of batch fabrication processes, the commodity cost will be much lower. Design changes can be implemented, and malfunctioning or damaged systems replaced rapidly and inexpensively. The deformable mirror system can be manufactured as a component of a modular adaptive optics system.

Thus, by using MEMS technology, the image resolution of an adaptive optical system can be improved while reducing weight, manufacturing time, actuator cost, and assembly complexity. In the following sections, we describe a preliminary research effort involving design, fabrication, and testing conducted at Boston University with the goal of producing a 400-element MEMS deformable mirror array.

### 4 Processing Technology

To fabricate test devices economically and with a reasonable turnaround time, the multiuser MEMS process (MUMPs) at the Microelectronics Center of North Carolina<sup>14</sup> was used. This is a three-layer polycrystalline silicon (polysilicon) surface micromachining process. A surface micromachining process typically uses alternating layers of polysilicon as the structural material, oxide as the sacrificial layers, and silicon nitride as an electrical isolation layer. Figure 3 shows a cross-sectional schematic view of a typical micromachined actuator with a portion of a mirror sheet over it. The first polysilicon layer is used for address pads and the others for the actuators and mirror respectively. Holes are patterned into the top two polysilicon layers to enable subsequent release by wet chemical etch of the sacrificial oxide layers. Using this basic design, several generations of single actuators as well as arrays of actuators with a mirror sheet over them have been designed, fabricated, and tested.

The principal requirements for the deformable mirror surface are planarity and continuity. All test devices fabricated so far have excessive nonplanarity on the mirror surface (on the order of the layer thicknesses) that arise from the conformity inherent in surface micromachining. The schematic in Fig. 3 illustrates this phenomenon clearly. Furthermore, the mirror in the test devices has holes to provide access for acid for a wet chemical etch to release the oxide layers. Holes on the mirror surface are detrimental; they trap light and cause undesired diffraction effects,

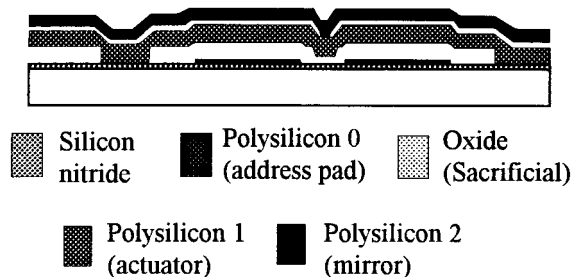


Fig. 3 Schematic of fabricated deformable mirror test structure using MUMPs.

having essentially the same effect as gaps in a segmented mirror. A possible solution to this problem is described below, and will be implemented in future prototypes.

Based on a design strategy developed in collaboration with MCNC, an acceptably planar surface can be obtained if all cuts in the underlying polysilicon layers are only 1.5  $\mu\text{m}$  wide. Fixed ends for the actuators as well as the attachment posts for the mirror can be built as honeycomb structures in order to keep to this requirement. Leaving the oxide inside the support structures will ensure adequate strength. Figure 4 is a schematic illustrating this design concept.

To release the structure, an anisotropic etch could be carried out from the back side of the silicon substrate at 1 to 2-mm spacing. The nitride could then be reactive ion (RIE) etched, and the 1.5- $\mu\text{m}$  holes and slots in the polysilicon layers would permit release of the oxide. This would eliminate the requirement for holes in the mirror for release etching of the oxide.

### 5 Actuator Design and Characterization

A principal indicator of expected MEMS mirror performance is the dynamic behavior of its constituent electrostatic actuators. Their repeatability, precision, frequency response, and robustness were quantified in an experimental and analytical research effort described below.

Actuator deflection was numerically simulated using a one-dimensional electromechanical model, illustrated in Fig. 5. This is a reasonable approximation since the structure has initially parallel components with a small gap compared with the lateral dimensions.<sup>15</sup> The diaphragm was modeled as a double cantilever beam, with a gap-dependent, electrostatic actuating force. Deflection is a function of applied electric field, material properties, and geometry.

From elasticity theory, the beam deflection  $y(x)$ , taking into consideration the electrostatic force and residual force is

$$\frac{d^4 y}{dx^4} + \frac{P}{EI} \frac{d^2 y}{dx^2} = \frac{q}{EI}, \tag{5}$$

with the boundary conditions being

$$y(0) = y(L) = 0, \quad y'(0) = y'(L) = 0,$$

where  $P$  is the axial force at the supports,  $E$  is the elastic modulus of the beam, and  $I$  is the moment of inertia of the

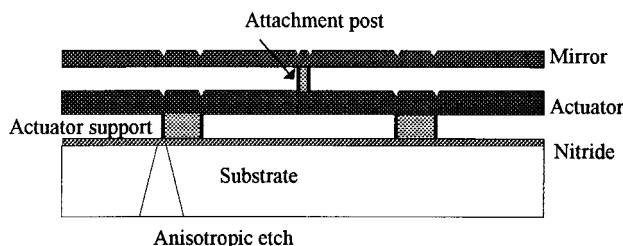


Fig. 4 Schematic of a new design for a continuous deformable mirror to achieve a planar mirror surface.

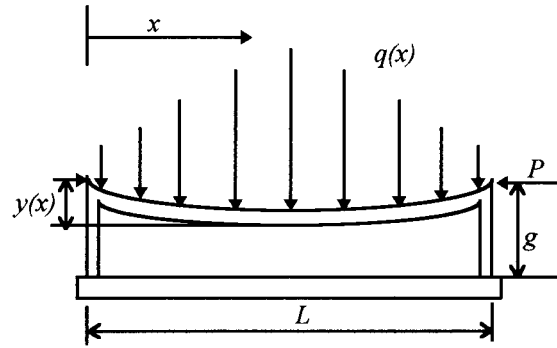


Fig. 5 Actuator model for analytical and numerical evaluation.

beam. From electrostatics, the distributed force,  $q$ , acting on the beam as a function of position along the beam is

$$q = \frac{\kappa^2 \epsilon_0 w}{2(g-y)^2} V^2, \tag{6}$$

where  $\kappa$  is the dielectric constant of the gap material,  $\epsilon_0$  is the permittivity of free space, and  $V$  is the applied voltage. This gives the fourth order nonlinear ordinary differential equation

$$\frac{d^4 y}{dx^4} + \frac{d^2 y}{dx^2} \frac{P}{EI} = \frac{\kappa^2 \epsilon_0 w}{2(g-y)^2} V^2. \tag{7}$$

This equation was numerically modeled using the shooting method, a standard technique for solving two-point boundary value problems. Figure 9 shows the numerically simulated deflection (normalized with gap) at the midpoint of the beam as a function of normalized voltage. These results were obtained for a compressive residual stress of 10 MPa. The results based on the numerical model are within 15% of the experimentally measured values of maximum deflection before pull-in and the critical voltage at which pull-in occurred. This model for an actuator is fast and reasonably accurate, and will be used in the more complex continuous mirror model.

Actuator geometry was based on theoretical and numerical calculations to optimize stroke and reduce the possibility of buckling due to residual stress. Within the framework of the restrictions imposed by the foundry process, several actuator geometries and shapes were fabricated and tested. Based on results from experiments with different geometries, fixed-fixed electrostatic actuators measuring 350  $\mu\text{m}$  square and 3.5  $\mu\text{m}$  thick with a 2.0- $\mu\text{m}$  actuator gap were chosen as the optimum design for test devices. Figure 6 shows the schematic of the described individual actuator.

The critical issues relating to device performance are yield (indicating process reliability), position repeatability, and frequency response. Previous MEMS research demonstrated that the average yield for individual microsensors and microactuators is 40 to 60%. Massively parallel, multiple microactuator systems implementing macroscopic functions require higher yields (greater than 90%) and designs with fault-tolerant function. Device yield is therefore a major concern, and experiments to characterize this have

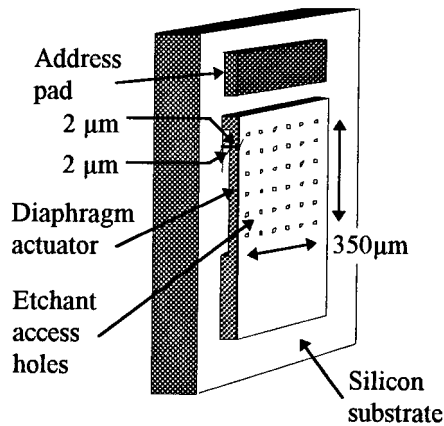


**Fig. 6** Schematic of an individual test actuator, showing optimum dimensions.

given optimistic results. A total of 487 individual actuators were tested in one study, with a yield of 94.5% useful, working actuators.

Preliminary device characterization was carried out by visual inspection under a Nomarski interference microscope. Figure 7 shows pictures of a single actuator when it is undeflected and when it has been pulled down by applying a voltage.

Deflections were measured using a single-point, split frequency, displacement-measuring laser interferometer. This device uses a focused laser beam to measure normal displacement with a position resolution of 2.5 nm and time resolution of 15.6 ns, a range of  $\sim 1$  mm, a frequency bandwidth of 0 to 133 kHz, and a lateral averaging area of several micrometers.

To actuate a diaphragm, voltage was applied between the address pad and the diaphragm using a pair of microprobes. When subjected to a voltage ramp (0 to 65 V), the deflection of the test actuator increased nonlinearly until the voltage reached 60 V, at which time it was deflected by approximately  $0.9 \mu\text{m}$ , shown by the dotted line in Fig. 8. Above this critical or pull-in voltage, the actuator would undergo the well-known electrostatic actuator phenomenon called “snap through instability,” instantaneously deflecting all the way to  $1.7 \mu\text{m}$ . When voltage was decreased from the measured critical voltage, the actuator remained in its snapped position until the voltage was decreased to 50 V, when it decreased nonlinearly following the path along which it had increased.

Figure 9 shows the measured and predicted response of two different actuators in the operating range, at voltages below pull-in voltage. The deflections have been normalized with a  $2\text{-}\mu\text{m}$  gap, and the voltage with the pull-in voltage characteristic of each curve. The numerical model assumes a residual stress of 10 MPa (compressive).

An extensive study was carried out to test the repeatability of the device position.<sup>16</sup> The motivation for a detailed study and statistical analysis of actuator behavior stems from the requirements for high repeatability and resolution in this application. This study will also pave the way for using MEMS devices in other applications where nanometer-scale control is required.

Over the desired actuation range, resulting in surface

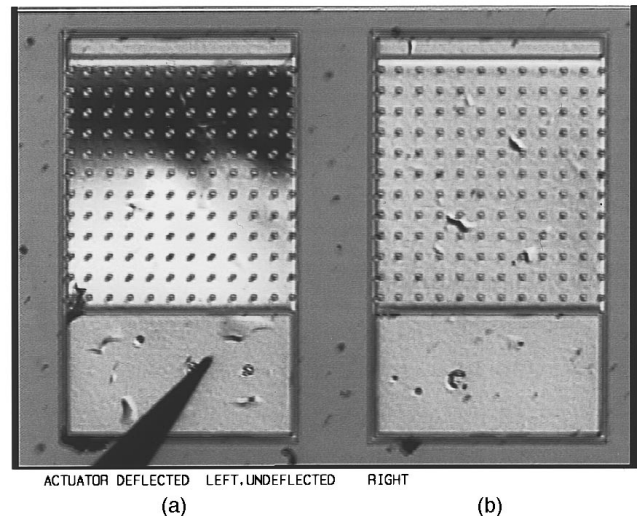


**Fig. 7** A single actuator viewed under a Normarski microscope at  $50\times$ . The actuator is undeflected at 0 V (a) and deflected at 60 V (b). The etch holes in the diaphragm are clearly visible.

normal actuation of 0 to 500 nm at the center of the cantilever, with maximum applied voltage less than pull-in voltage, there was no hysteresis and an average position repeatability of 9.76 nm (for a 99% confidence level) was obtained, as shown in Fig. 10.

Figure 11 shows the amplitude response of an actuator. The actuators were found capable of responding to frequencies of up to 66 kHz (Nyquist frequency of the measurement system) without attenuation. The actuators drew no measurable current, which implies that the array is thermodynamically reversible, as expected for an electrostatic system. There was no electrical coupling between actuators.

## 6 Fabrication and Control of Mirror Arrays

Parallel arrays of surface-normal electrostatic actuators with segmented mirrors were designed, built, and tested. A 16-element segmented mirror array was wire bonded to a

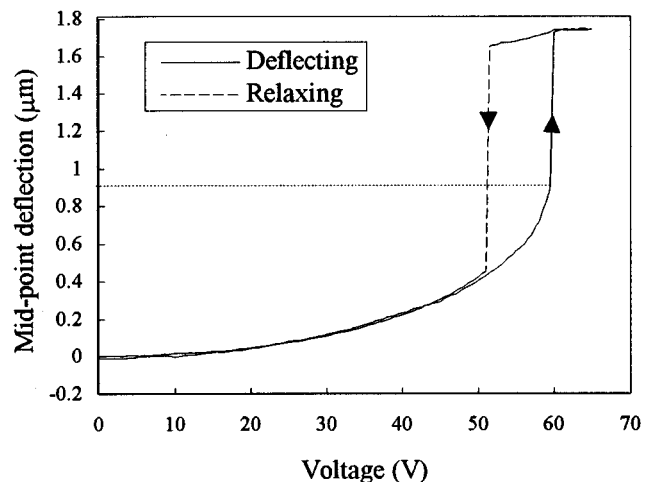


**Fig. 8** Measured deflection as a function of increasing and decreasing voltage.

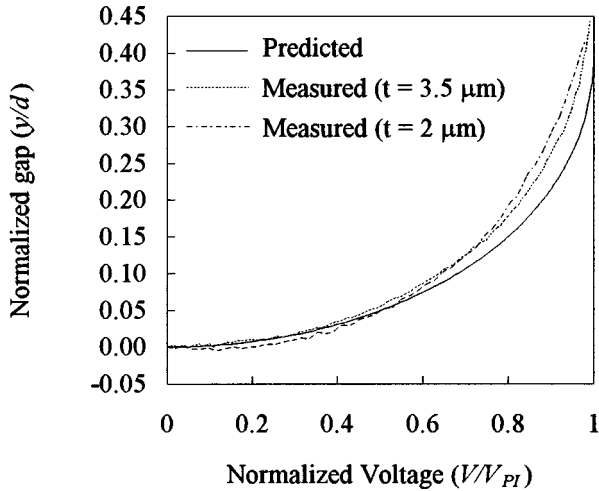


Fig. 9 Predicted and measured deflections for two 350- $\mu\text{m}$  square actuators with different thicknesses.

standard 64-pin dual in-line package (DIP), from which connections can be made to a control interface. Figure 12 shows a photograph of the mirror array wire bonded to a chip carrier and mounted on a PC board.

Actuator characterization suggested that the actuators in a given array could be used in an open-loop actuation control scheme, provided that each actuator's response was previously characterized. Dedicated support circuitry has been developed for the MEMS mirror systems, focusing on the design of a circuit capable of simultaneously driving a large number of actuators under computer control. A 20-channel circuit has been designed and fabricated. The circuit contains a computer interface board addressable via C software. The 20 separate channels each consist of a parallel-loaded digital-to-analog integrated circuit and a high-voltage driving circuit. The circuit has been designed so that it can be expanded to drive up to 400 actuators simultaneously.

The drive electronics are low power, and inexpensive as a result. The high-voltage driver must be capable of with-

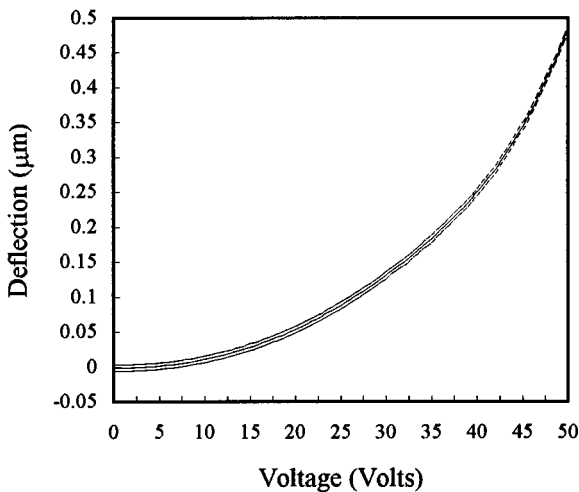


Fig. 10 Position repeatability of a single actuator.

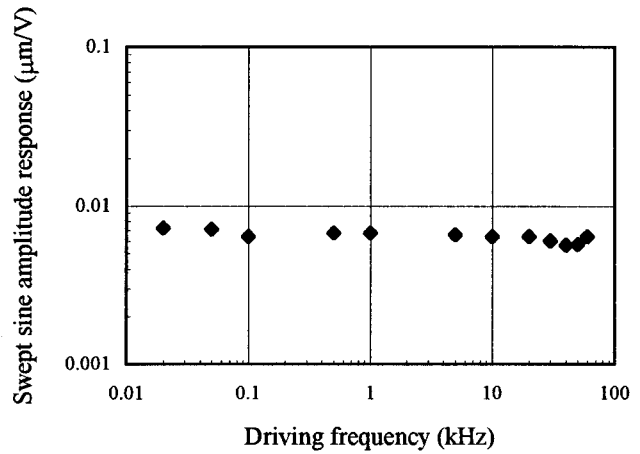


Fig. 11 Amplitude response of a microactuator. The sinusoidal drive voltage was 26.3 V (peak-to-peak) with a 10 V dc offset, resulting in 200  $\mu\text{m}$  of maximum deflection.

standing output short circuits in the event of actuator failure, must have bandwidth sufficient to enable real-time actuator control, and must be easy to reproduce in compact, miniature form. A working version of a suitable driver module has been designed and tested using readily available, off-the-shelf operational amplifiers and transistors. The current prototype uses only a small number of components and can produce voltages up to 400 V with a 10-kHz bandwidth.

### 7 Conclusions

Silicon micromachined deformable mirrors represent a high-performance, low-cost technology for enhancing image resolution. This paper describes the initial development of a MEMS deformable mirror, focusing on design, fabrication, device characterization, and system integration issues. The mirror parameters were developed based on theoretical and empirical models of adaptive optics. Sufficient yield was demonstrated with a standard, robust actuator.

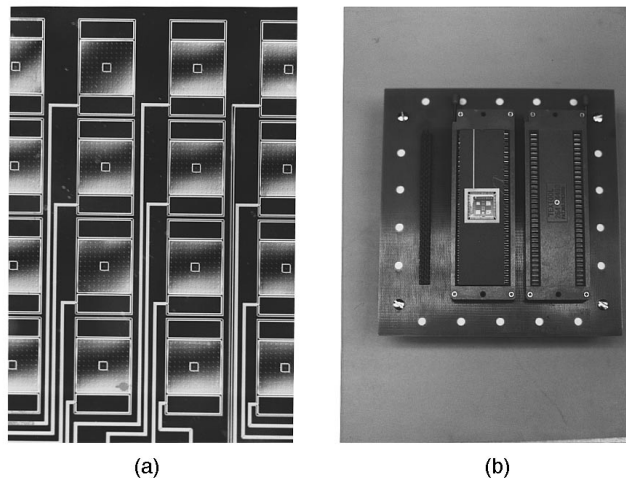


Fig. 12 (a) Optical micrograph of a 16-element segmented mirror and (b) Photograph of wafer wire bonded to a standard 64-pin chip carrier.

Extensive statistical actuator characterization demonstrated remarkable performance levels with regard to repeatability and bandwidth. Processing issues for obtaining a planar mirror surface are currently being addressed. A 20-channel electronics control circuit has been built and used for high-speed control of a segmented mirror array.

### Acknowledgments

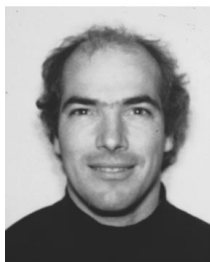
This research is being funded by a 3-year contract with DARPA (DABT63-95-C-0065), and was initiated on a Small Grant for Exploratory Research from the National Science Foundation (DDM9317937). We are grateful to the staff at the Microelectronics Center of North Carolina for their generous assistance. Thanks to Dr. David Castañón for his valuable suggestions. Thanks also to Adam Maines, Larry DePaulis, and Laura Rennie.

### References

1. J. M. Younse, "Mirrors on a chip," *IEEE Spectrum* **30**(11), 27–31 (1993).
2. D. A. Gregory, R. D. Juday, J. Sampson, R. Gale, R. W. Cohn, and S. E. Monroe, "Optical characteristics of a deformable-mirror spatial light modulator," *Opt. Lett.* **13**(10), 10–12 (1988).
3. J. M. Florence and R. O. Gale, "Coherent optical correlator using a deformable mirror device spatial light modulator in the Fourier plane," *Appl. Opt.* **27**(11), 2091–2093 (1988).
4. J. L. Horner and P. D. Gianino, "Phase-only matched filtering," *Appl. Opt.* **23**(6), 812–816 (1984).
5. G. Vdovin and P. M. Sarro, "Flexible mirror micromachined in silicon," *Appl. Opt.* **34**, 2968–2972 (1995).
6. G. Vdovin, "Spatial light modulator based on the control of the wavefront curvature," *Opt. Comm.* **115**, 170–178 (1995).
7. L. M. Miller, M. L. Argonin, R. K. Bartman, W. J. Kaiser, T. W. Kenny, R. L. Norton, and E. C. Vote, "Fabrication and characterization of a micromachined deformable mirror," *Proc. SPIE* **1945**, 421–430 (1993).
8. J. W. Hardy, "Adaptive optics: a new technology for the control of light," *Proc. IEEE* **66**(6), 651–697 (1978).
9. J. E. Pearson and S. Hansen, "Experimental studies of a deformable-mirror adaptive optical system," *J. Opt. Soc. Am.* **67**(3), 325–333 (1977).
10. R. J. Tyson, *Principles of Adaptive Optics*, Academic Press, San Diego, CA (1990).
11. B. Hulburd and D. Sandler, "Segmented mirrors for atmospheric compensation," *Opt. Eng.* **29**(10), 1186–1190 (1990).
12. E. Steinhaus and S. G. Lipson, "Bimorph piezoelectric flexible mirror," *J. Opt. Soc. Am.* **69**(3), 478–481 (1979).
13. M. A. Ealey and J. F. Washeba, "Continuous facesheet low voltage deformable mirrors," *Opt. Eng.* **29**(10) (1990).
14. D. A. Koester, R. Mahadevan, and K. W. Markus, "MUMPS Introduction and Design Rules," MCNC Technology Applications Center, 3021 Cornwallis Rd, Research Triangle Park, NC (1994).
15. P. Osterberg, H. Yie, X. Cai, J. White, and S. Senturia, "Self-consistent simulation and modeling of electrostatically deformed diaphragms," *Proc. MEMS 1994*, pp. 28–32 (1994).
16. R. Krishnamoorthy, T. G. Bifano, and G. Sandri, "Statistical performance evaluation of electrostatic micro actuators for a deformable mirror," *Proc. SPIE* **2881**, 35–44 (1996).



**Raji Krishnamoorthy Mali** received a BS (1992) in mechanical engineering from the University of Bombay, India. She was a Presidential University Graduate Fellow at Boston University and received an MS in mechanical engineering in 1994. She is currently a doctoral student at Boston University, and is involved in the development of a surface micromachined deformable mirror for adaptive optics applications.



**Thomas G. Bifano** received BS (1980) and MS (1983) degrees in mechanical engineering and materials science from Duke University and a PhD (1988) in mechanical engineering from North Carolina State University. Since joining the faculty of Boston University in 1988, he has developed an internationally known research program to study ultraprecision machining. He directs the Boston University Precision Engineering Research Laboratory, where he oversees projects on ion machining of ceramics, ceramic hard-disk substrate fabrication, and silicon micromachining of deformable mirror systems.



**Nelsimar Vandelli** received a BS in mechanical engineering from the Military Institute of Engineering, Brazil, in 1986. He worked at the Brazilian Petroleum Co. from 1987 to 1991, when he joined the graduate program at Boston University. He is pursuing a doctoral degree in mechanical engineering. His research involves finite-element analysis of microelectromechanical devices.



**Mark N. Horenstein** received his BS and PhD degrees in electrical engineering from the Massachusetts Institute of Technology in 1973 and 1978, respectively, and his MS degree in electrical engineering from the University of California at Berkeley in 1975. From 1978 to 1979, he was a research scientist and development engineer for Spire Corporation in Bedford, Massachusetts. In 1979, he joined the faculty in the Department of Electrical and Computer Engineering at Boston University where he now continues as Associate Professor. He specializes in the field of electrostatics and its application to problems in research and industry. He is the author of numerous papers on topics in electrostatics, including the development of electric field and ion measuring instrumentation, the use of air ions to neutralize moving webs and fabrics, the effects of electrostatic charge on the opening of parachutes, and the use of ions to detect defects in barrier membranes. He also holds several patents related to electrostatic devices and processes. He joined the Boston University MEMS team in 1995.